

Attention-Augmented Inverse Reinforcement Learning with Graph Convolutions for Multi-Agent Task Allocation

Huilin Yin, Zhikun Yang, Linchuan Zhang, Daniel Watzenig

Abstract—Multi-agent task allocation (MATA) plays a vital role in cooperative multi-agent systems, with significant implications for applications such as autonomous vehicle coordination, intelligent vehicular logistics and cooperative robotics in transportation systems. Although traditional deep reinforcement learning (DRL) methods have been shown to be promising, their effectiveness is hindered by a reliance on manually designed reward functions and inefficiencies in dynamic environments. In this paper, an inverse reinforcement learning (IRL)-based framework is proposed, in which multi-head self-attention (MHSA) and graph attention mechanisms are incorporated to enhance reward function learning and task execution efficiency. Expert demonstrations are utilized to infer optimal reward densities, allowing dependence on handcrafted designs to be reduced and adaptability to be improved. The proposed framework demonstrates notable effectiveness in optimizing cumulative rewards and improving coordination efficiency, as validated through extensive experimentation.

Index Terms—Multi-agent task allocation, multi-agent reinforcement learning, inverse reinforcement learning.

I. INTRODUCTION

WITH advancements in automatic control, computer technology and artificial intelligence, Multi-Agent Systems (MAS) have attracted increasing attention [1]. As an extensively studied and applied subfield, MAS enables multiple agents to complete tasks cooperatively [2]. In domains such as logistics, search and rescue, the workload and complexity often exceed the capabilities of single agents [3]. MAS address these challenges by offering greater flexibility, fault tolerance, and robustness [4]. A representative application is warehouse automation using Automated Guided Vehicles (AGVs), where coordinated operation among multiple AGVs is crucial for efficient material handling and distribution. However, realizing efficient collaboration in MAS relies heavily on effective task allocation.

As shown in Fig. 1, multi-agent task allocation (MATA) is a fundamental issue in MAS research. The quality of task allocation directly affects the system’s operational efficiency. When task complexity exceeds the capability of a single agent, enabling cooperation among agents becomes essential

This work has been submitted to the IEEE for possible publication. Copyright may be transferred without notice, after which this version may no longer be accessible.

Huilin Yin and Zhikun Yang are with the College of Electronic and Information Engineering, Tongji University, Shanghai 200092, China (e-mail: yinhuilin@tongji.edu.cn; xiaoyuezk@tongji.edu.cn).

Linchuan Zhang is with the Shanghai Research Institute for Intelligent Autonomous Systems, Tongji University, Shanghai 201210, China (e-mail: jmzlc@tongji.edu.cn).

Daniel Watzenig is with the Graz University of Technology and also with the Virtual Vehicle Research GmbH, 8010 Graz, Austria (e-mail: daniel.watzenig@tugraz.at).



Fig. 1. Schematic diagram of MATA for AGV formation.

[5]. Practical applications impose diverse demands on task allocation methods. Traditional optimization-based methods such as G-CBBA [6] and ImprovedQPSO [7] have achieved notable success in small-scale, static environments. However, MATA is an NP-hard problem [8] and these methods struggle with scalability, adaptability, and real-time requirements in large-scale, dynamic settings [9].

To address these limitations, deep reinforcement learning (DRL) methods have been applied to MATA. DRL allows agents to autonomously acquire policies by interacting with dynamic environments, offering greater adaptability to uncertainty. Unlike traditional methods, DRL exhibits superior adaptability in dynamic and uncertain scenarios [10]. DRL-based methods effectively address the limitations of traditional algorithms, significantly improving multi-agent task coordination in complex and dynamic vehicular systems, enhancing operational efficiency and robustness.

Despite advancements in DRL, most existing approaches still rely heavily on manually designed reward functions, which are often difficult and subjective to define accurately in complex task allocation scenarios. Moreover, agents struggle to balance exploration and exploitation without sufficient prior knowledge [11]. To address these issues, inverse reinforcement learning (IRL) has been explored, particularly in robot path planning. IRL infers reward functions from expert demonstrations, eliminating the need for manual design. Techniques such as Maximum Entropy IRL and Feature Expectation Matching have successfully derived implicit objectives for complex planning tasks [12], [13], enabling robust decision-making in dynamic environments.

Although MATA is more complex—featuring dynamic tasks and inter-agent coordination—it shares core challenges with path planning, such as sequential decision-making and global optimization. Nevertheless, IRL research in MATA remains scarce. Most existing studies focus on algorithmic performance, while the integration of global information and prior knowledge into multi-agent learning remains underexplored

[14], [15].

Motivated by the success of IRL in path planning, an IRL-based framework is extended to the MATA setting to address the challenges of reward function design and agent coordination in complex environments. To improve reward modeling and decision-making, multi-head self-attention (MHSA) and graph attention networks (GAT) are incorporated. MHSA is utilized to capture intricate dependencies within agent trajectories, while GAT is employed to model global agent-task relationships through graph-structured state representations. Through these mechanisms, more expressive feature representations and robust reward estimations are enabled, enhancing the overall efficiency and adaptability of task allocation.

The primary contributions of this study are as follows.

- 1) An attention-enhanced IRL framework is proposed to alleviate DRL's dependence on manual reward design. By leveraging the MHSA mechanism, the framework effectively extracts trajectory features and enhances reward functions using expert trajectory data, thereby improving task allocation efficiency.
- 2) A global information feature extraction module based on hierarchical graph convolutional networks is developed. This module optimizes reward allocation and regulation in the IRL generator. By capturing global interdependencies among agents and tasks, it efficiently models agent-task interactions in complex scenarios, enhancing global coordination in task allocation.
- 3) Extensive experiments demonstrate the effectiveness of the proposed framework across different scales. The framework is evaluated under varying task scales with a fixed number of agents and under varying agent scales with a fixed number of tasks. Experimental results show that the proposed method effectively enhances reward efficiency and coordination quality in MATA.

The remainder of the paper is organized as follows. Section II reviews related work. Section III describes the MATA system model and problem formulation. Section IV presents the proposed approaches. Section V describes the experiments and results. Finally, Section VI concludes the paper.

II. RELATED WORK

This section reviews existing works that utilize DRL to address the MATA, including centralized and distributed approaches. Additionally, this section also reviews research on IRL conducted in other fields.

A. DRL based task allocation

Multi-agent reinforcement learning (MARL) can be categorized in various ways based on different characteristics. According to the training and execution methods, it can be classified into Centralized Training and Centralized Execution (CTCE), Centralized Training and Decentralized Execution (CTDE), and Decentralized Training and Decentralized Execution (DTDE) [16].

In [17], task graphs are normalized to eliminate spatial distortions (translation, scaling, rotation), enhancing adaptability to diverse maps while maintaining computational efficiency. In

[18], action spaces are pre-constrained via task pre-allocation, accelerating inference and improving performance in dynamic scenarios, with notable zero-shot generalization to unseen tasks. Although CTCE methods can theoretically approach globally optimal strategies, they rely on centralized controllers during execution. This makes them vulnerable to single points of failure and impractical in real-world deployments.

In the CTDE paradigm, decentralized decisions are made after centralized training, offering robustness against communication failures and improved scalability. Various approaches have been developed under this framework. CapAM [19] combines capsule networks with attention-based GNNs to capture local and global features of task graphs, maintaining performance as task-agent scales increase. An auction-based RL framework [14] coordinates agents through proposer-responder roles, enabling fast decision-making in dynamic environments. Hierarchical reinforcement learning [20] decomposes tasks into subchains, using QMIX-based value decomposition to ensure effective collaboration. To address practical constraints in real-world scenarios, more recent methods have incorporated advanced architectures and application-specific adaptations. LIA-MADDPG [21] enhances robot swarm coordination by aggregating local information during distributed execution. In cooperative transport [22], task priorities are integrated with global communication to support coordination under partial observability. MAGNET [23] embeds GNNs into the CTDE structure to achieve scalable, conflict-free task assignment among autonomous vehicles. In UAV-assisted mobile crowd sensing [24], task allocation and trajectory planning are jointly optimized using a CTDE-based MARL framework with integrated greedy strategy to enhance coverage efficiency.

In the DTDE paradigms, both training and execution are performed independently by each agent, ensuring robustness in highly dynamic or communication-limited environments. The HIPPO-MAT framework [25] integrates GraphSAGE-based GNNs with Independent PPO, enabling heterogeneous agents to process local observations and allocate tasks autonomously without central coordination. GAPPO [26] combines genetic algorithms with PPO to enhance agent adaptability, allowing agents to dynamically adjust task assignments based on local evaluations, leading to improved efficiency and reduced completion time.

Most existing MARL methods require agents to learn optimal policies through extensive interaction with the environment, leading to high sample complexity and prolonged training times, especially in sparse-reward or high-dimensional settings. In addition, their reliance on manually designed reward functions limits adaptability in complex and dynamic MATA scenarios.

B. Studies of IRL Methods

IRL has been widely applied in tasks such as path planning and target search, where expert behavior is observable but the underlying reward functions are not explicitly defined. For instance, IRL has been used to reconstruct cost functions in cooperative multi-vehicle planning [27] and to jointly solve path planning and power allocation problems with improved generalization over behavioral cloning [13].

To enhance reward modeling, several studies incorporate structural priors into IRL frameworks. Maximum entropy IRL with submodular functions [12] exploits diminishing marginal returns to maintain consistent search performance. Adaptive submodular IRL [28] further introduces coverage-based exploration to improve spatial efficiency in dynamic environments. In [29], hierarchical transformers and MaxEnt IRL are combined for motion forecasting, using cross-attention and occupancy maps to model context-aware rewards and generate feasible, multimodal trajectories.

IRL has also been extended to offline and cross-domain contexts. Bundle Behavior Cloning [30] segments expert trajectories temporally to improve policy learning under non-stationary dynamics. A query-based offline IRL approach [31] has been applied to prompt optimization in large language models, learning reward structures from past interaction logs to reduce online training cost.

More recently, IRL has been extended to explicitly multi-agent settings. The MIRL framework in [32] introduces entropy-regularized games to ensure equilibrium uniqueness and improve interpretability, supported by theoretical analysis of estimation error and sample complexity. In [33], an off-policy MIRL algorithm recovers individual reward signals from collective behaviors, such as fish schooling and microbial colonies, using ReF-ER and guided cost learning. Inverse game-theoretic formulations have also been explored. In [34], MIRL is framed as a generative-adversarial optimization task, and polynomial-time algorithms are proposed with strong performance in real-world settings like electricity market prediction.

Collectively, these studies demonstrate IRL's strong capability in inferring meaningful reward structures from expert behavior, even in sparse, high-dimensional or partially observable environments. However, most existing methods are tailored to single-agent settings or assume full observability. Applications of IRL in multi-agent task allocation (MATA) remain limited, particularly in scenarios requiring coordinated behavior, global state abstraction and reward learning from decentralized demonstrations. These gaps highlight the need for IRL frameworks specifically designed to address the unique challenges of MATA.

III. SYSTEM MODEL AND PROBLEM FORMULATION

To support efficient and conflict-free task allocation in the MATA setting, key assumptions and constraints on agent behavior, task timing, and energy consumption are defined in the system model. Based on these formulations, an optimization problem is constructed to capture the trade-offs between energy usage and task completion efficiency.

A. System Model

This study considers a MATA scenario common in logistics and emergency response, featuring multi-task agents with single-task assignment and instantaneous allocation. In this scenario, each task requires only one agent for completion and is removed upon completion. Agents perform multiple

tasks sequentially until all tasks are completed. No priority or mandatory dependency exists among tasks.

In the MATA framework, the agent set of N agents is denoted as $\Lambda = \{\lambda_1, \lambda_2, \dots, \lambda_i, \dots, \lambda_N\}$, and the task set of M tasks is denoted as $J = \{j_1, j_2, \dots, j_k, \dots, j_M\}$, where $n < M, i < N, j < M$. All tasks are predefined and remain fixed during execution. The agent set is homogeneous, meaning each agent can complete any task. This design avoids the complexity of handling heterogeneous capabilities and ensures an equal opportunity for task assignment among agents. Task allocation is represented by $C : J \rightarrow \Lambda$. If task j_k is assigned to agent λ_i , then $C_{ki} = 1$; otherwise, $C_{ki} = 0$.

The following notations are used: $Z = \{z_1, z_2, \dots, z_M\}$ for task start times, $O = \{o_1, o_2, \dots, o_M\}$ for task waiting times, and $G = \{g_1, g_2, \dots, g_M\}$ for task durations. For any two tasks j_u and j_v ($u \neq v$) assigned to the same agent, the combined end time of one task must not interfere with the start time of the other. This requires that either $z_u + o_u + g_u \leq t_v$, meaning task j_u finishes before task j_v starts, or $z_v + o_v + g_v \leq t_u$, meaning task j_v finishes before task j_u starts. Both conditions ensure sequential task handling without time conflicts.

Define the sequence of coordinate pairs $Traj_{ki} = [(x_1, y_1), (x_2, y_2), (x_3, y_3), \dots, (x_l, y_l)]$ with a length of L as the trajectory traversed by agent λ_i while transitioning from the completion of its previous task to the execution of task j_k . Then the moving distance of this process is $\sum_{d=1}^{L-1} \left\| Traj_{ki}^{(d+1)} - Traj_{ki}^{(d)} \right\|_2$.

The following performance metrics are used to evaluate MATA performance:

$$\min \sum_{j_k \in J} \sum_{\lambda_i \in \Lambda} \sum_{d=1}^{L-1} \left\| Traj_{ki}^{(d+1)} - Traj_{ki}^{(d)} \right\|_2, \quad (1)$$

$$\min \sum_{j_k \in J} O_k. \quad (2)$$

Metrics (1) and (2) represent minimizing travel distance and minimizing waiting time respectively. These indicators reflect different aspects of efficiency. Their importance varies depending on the application.

B. Problem Formulation

Let $t_{\text{total}} = \max_{j_i \in J} (z_i + o_i + g_i) - \min_{j_k \in J} (z_k)$ represent the total elapsed time since task allocation began. Let the total energy of each robot be E , which decreases over time. The energy consumed during movement is denoted as E_c , and the energy consumed to complete task $j_k \in J$ is denoted as e_k . To simplify the constraint formula, we introduce the following auxiliary variables: $\theta_{uv} = \sum_{\lambda_i \in \Lambda} C_{ui} C_{vi}$, $\rho_k = z_k + o_k + g_k$. θ_{uv} is an indicator variable that denotes whether tasks j_u and j_v are assigned to the same agent. ρ_k represents the completion time of the task j_k .

The problem is defined as the following mixed-constraint optimization problem:

$$\min \alpha \sum_{\lambda_i \in \Lambda} \left(E_c - \sum_{j_k \in J} e_k \cdot C_{ki} \right) + \beta t_{\text{total}} \quad (3a)$$

$$\text{s.t.} \sum_{\lambda_i \in \Lambda} C_{ki} = 1, \quad \forall j_k \in J \quad (3b)$$

$$\forall u, v \in \{1, 2, \dots, M\}, u \neq v: \quad (3c)$$

$$\theta_{uv} ((\rho_u \leq z_v) \vee (\rho_v \leq z_u)) = \theta_{uv} \quad (3c)$$

$$E - E_c - \sum_{j_k \in J} e_k \cdot C_{ki} \geq 0, \quad \forall \lambda_i \in \Lambda, \quad (3d)$$

where α and β are non-negative coefficients. Objective function (3a) aims to balance two key objectives: maximizing remaining energy and minimizing task completion time. Maximizing the remaining energy after task completion extends system operation time and enhances resource utilization, while minimizing total completion time ensures task execution efficiency. The weights of these objectives are controlled by α and β , where α emphasizes energy conservation and β emphasizes time efficiency. These weights can be adjusted based on application scenarios to optimize performance.

Constraint (3b) ensures that each task $j_k \in J$ must be assigned to exactly one agent $\lambda_i \in \Lambda$, preventing tasks from being omitted or redundantly assigned. This constraint reflects the physical requirement that each task is a single-agent task requiring a clear and unique responsibility allocation. Constraint (3c) ensures that each agent can only perform one task at any given time, avoiding scheduling conflicts. If two tasks j_u and j_v are assigned to the same agent, their execution times must not overlap. Constraint (3d) limits the energy consumption of agents. The remaining energy of each agent is the initial total energy E minus the total energy consumed in performing tasks. The remaining energy is required to be non-negative to ensure that the agent will not fail due to energy exhaustion during task execution.

IV. PROPOSED APPROACHES

In this section, the system model and problem formulation introduced in Section III are reformulated as a Markov Decision Process (MDP). Building on this framework, an efficient algorithm based on IRL is developed to effectively address the MATA.

A. DRL based Task Allocation

In general, reinforcement learning is modeled as a sequential decision-making method based on the framework of a MDP. A MDP is typically represented as a tuple $\langle S, A, T, R, \gamma \rangle$, where the state at time $t+1$ depends only on the state at time t and is independent of the state at $t-1$. The components are defined as follows:

- S : A finite state space.
- A : A finite action space.
- P : The transition function, defined as $P : A \times S \rightarrow S$, representing the probability of transitioning to the next state $S(t+1) = s_{t+1}$ from the current state $S(t) = s_t$ under action $A(t) = a_t$.

- R : The reward function, defined as $R : S \times A \rightarrow \mathbb{R}$, representing the expected reward $R(t+1) = r_{t+1}$ under state $S(t) = s_t$ and action $A(t) = a_t$.
- γ : The discount factor, which determines the present value of future rewards by applying a decay to rewards over time.

A policy π is defined as a computable function that maps each state $S(t) = s_t$ to an action $A(t) = a_t$, i.e., $\pi : S \rightarrow A$. It represents the agent's decision-making strategy within the MDP framework.

In this paper, it is assumed that each agent independently determines its own actions to maximize its discounted future rewards. The immediate reward obtained by each agent during the training process depends on its position and coordination. The designs of the state space S , action space A and reward function R are as follows:

State Space S : In smart transportation and vehicular logistics scenarios, an individual agent's perception via vision or LiDAR is limited. However, reliable communication enables agents to share global state information, including the positions of agents and tasks, ensuring equal access to a comprehensive state representation.

Action Space A : As homogeneous agents with identical characteristics, all agents share the same action space, consisting of movement distance and direction. To simplify the problem, a uniform movement speed can be assumed, reducing the action space to movement direction only. The joint action of all agents is denoted as $\mathbf{a}_t = (a_{1,t}, a_{2,t}, \dots, a_{N,t})$, with corresponding joint policies $\boldsymbol{\pi}_t = (\pi_{1,t}, \pi_{2,t}, \dots, \pi_{N,t})$.

Reward Function R : Based on the objective function (3a), the reward balances energy consumption and task efficiency. Assuming uniform energy consumption per unit distance, let $d_{i,t}$ denote the distance moved by agent λ_i at time step t . The corresponding energy consumption is given by $E_c = f(d_{i,t})$, where $f(*)$ maps distance to energy cost. Although E_c reflects actual energy use, it is often difficult to measure precisely in practice, whereas distance $d_{i,t}$ and time t are readily observable. Therefore, the reward function is then formulated as a weighted combination of energy consumption with coefficient η and task efficiency with coefficient ϕ :

$$r_{i,t} = \eta f(d_{i,t}) + \phi t. \quad (4)$$

In Multi-agent DRL, the expected return $J_i(\pi_i)$ of each agent is maximized based on the maximum entropy principle:

$$J_i(\pi_i) = \mathbb{E}_{\tau \sim \pi} \left[\sum_{t=0}^{\infty} \gamma^t r_{i,t}(s_t, \mathbf{a}_t) \right], \quad (5)$$

where $r_{i,t}(s_t, \mathbf{a}_t)$ represents the immediate reward for agent λ_i . Since the state transition is determined by the joint action \mathbf{a}_t , the reward for a single agent also depends on the joint action.

Multi-agent DRL includes the action-value network and policy network. The action-value function $Q_i(s_t, \mathbf{a}_t)$ for each agent λ_i is defined as:

$$Q_i(s_t, \mathbf{a}_t) = \mathbb{E}_{\tau \sim \pi} \left[\sum_{k=0}^{\infty} \gamma^k r_{i,t}(s_{t+k}, a_{i,t+k}) \middle| s_t, \mathbf{a}_t \right]. \quad (6)$$

and β for modifying the reward function: $[\alpha, \beta]^T = W_r \cdot \frac{1}{L} \sum_{v=1}^L H_{ki}^{(v)} + b_r$, where $W_r \in \mathbb{R}^{2 \times d}$ and $b_r \in \mathbb{R}^2$ are the projection matrix and bias, respectively. And $H_{ki}^{(v)} \in \mathbb{R}^d$ denotes the v -th row of the matrix H_{ki} , corresponding to the feature representation at position v . After completing the generation process, the modified reward function is obtained:

$$r_i^{IRL} = \alpha r_i + \beta. \quad (11)$$

Unlike many existing methods [30], this study retains the use of manually designed functions. This approach provides the neural network with an initial reasonable direction, reducing the time spent exploring unnecessary strategies during the learning process. Additionally, it offers a stable baseline, reducing dependency on data quality and enhancing system robustness.

In the adversarial phase, as shown in the blue-shaded area in Fig. 2, an n -layer FCN is used as the discriminator. The discriminator is trained with binary cross-entropy loss, utilizing the true labels of the trajectories: expert trajectories are labeled as 1, while generated trajectories are labeled as 0. The discriminator outputs the probability of a trajectory being classified as an expert trajectory:

$$P_{ki} = \sigma(W_n \sigma(W_{n-1} \dots (W_1 \tau + b_1) + b_{n-1}) + b_n), \quad (12)$$

where $\sigma(*)$ is the non-linear activation function, and W_i and b_i are the weight matrix and bias vector for the i -th layer.

The loss function for the generator is:

$$\mathcal{L}_{gen} = -\mathbb{E}_{Traj_{ki}} [\log P_{ki}]. \quad (13)$$

The loss function for the discriminator is:

$$\mathcal{L}_{disc} = -\mathbb{E}_{Traj_{exp}} [\log P_{exp}] - \mathbb{E}_{Traj_{ki}} [\log(1 - P_{ki})]. \quad (14)$$

By minimizing the binary cross-entropy loss, the discriminator learns to accurately classify expert trajectories while distinguishing them from generated trajectories. This feedback serves as a critical learning signal for the generator, guiding it to iteratively refine its output to better mimic expert behavior, as shown by the data paths composed of green arrows in Fig. 2. Through this adversarial interaction, the training process is progressively driven toward convergence.

C. Global Information Feature Extraction

Traditional IRL primarily relies on agent trajectory data, overlooking global state information that is often crucial in cooperative or competitive multi-agent scenarios. This limitation can lead to suboptimal policy learning, especially when agent interactions are influenced by shared environmental dynamics. By integrating global states, the generator can simultaneously capture local behaviors and contextual environmental features, enabling the extraction of richer and more discriminative feature representations that better align with the true reward structure. As a result, the learned policy demonstrates enhanced consistency with expert behaviors and improved generalization capability when applied to complex and dynamic tasks.

The core of global state information lies in the interaction relationships between agents and tasks, as well as among

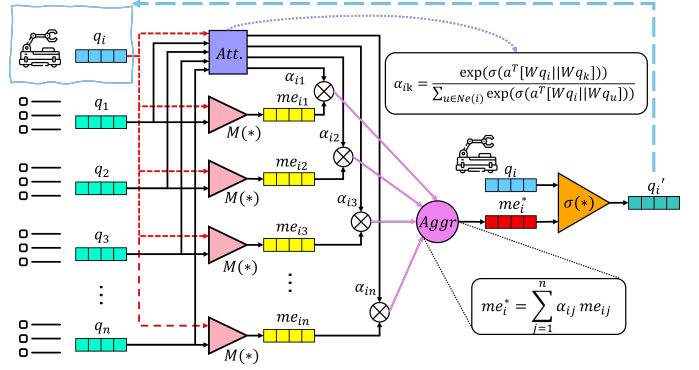


Fig. 3. Graph attention structure diagram.

agents. This includes the positions, states, and relative relationships of agents and tasks, which are well-suited to be represented as nodes and edges in a graph. Additionally, graph structures can flexibly adapt to the dynamic nature of multi-agent systems; by adding or removing nodes/edges, they can reflect changes in the environment or tasks. Therefore, the global state information is modeled as a graph: each agent and each task is represented as a node, and edges exist between agents and unfinished tasks. There are no edges connecting agents to agents or tasks to tasks.

As shown in Fig. 3, for agent λ_i at a given iteration, its feature vector is q_i . The feature vector q_i and the feature vector q_k of task j_k are processed through a message generation function $M(*)$ to produce the message $me_{ik} = M(q_i, q_k)$. Simultaneously, q_i and q_k are processed through an attention mechanism to generate the attention weight α_{ik} :

$$\alpha_{ik} = \frac{\exp(\sigma(a^T [Wq_i || Wq_k]))}{\sum_{u \in Ne(i)} \exp(\sigma(a^T [Wq_i || Wq_u]))}, \quad (15)$$

where $||$ denotes feature concatenation. W is a learnable linear transformation matrix used to map node features into a new feature space. $\sigma(*)$ is the non-linear activation function. $Ne(i)$ the set of neighbor nodes of node i . Each message is aggregated with attention weights to obtain the aggregated message me_i^* . After message aggregation, the feature vector is updated sequentially as follows:

$$q_i' = \sigma(q_i, me_i^*) = \sigma\left(q_i, \sum_{u \in Ne(i)} \alpha_{iu} me_{iu}\right). \quad (16)$$

As shown by the data paths composed of black and red arrows in Fig. 2, the global information feature extraction module is incorporated into the generator in a hierarchical manner. The agent trajectory information and global state information are processed sequentially through MHSA and graph attention to obtain preliminary feature information. The preliminary feature information is then concatenated and processed again using MHSA to produce the coefficients for the modified reward function.

D. Algorithm Description

In this section, the operational details of the proposed method are briefly introduced, and the pseudo-code is outlined

Algorithm 1 Train Multi-Agent System IRL

INPUT: number of training episodes N_{max} , number of steps in an episode t_{max} , learning rate of agents η , discount factor γ , batch size \mathcal{B} , replay buffer \mathcal{D} , number of heads H , model dimensionality d , learning rate of discriminator η^d

- 1: **for** $i = 1$ to N **do**
- 2: Initialize the agent with parameters η
- 3: **end for**
- 4: Initialize the generator with parameters H, d
- 5: Initialize the discriminator with parameters η^d
- 6: **for** $episode = 1$ to N_{max} **do**
- 7: Reset the environment
- 8: **for** $t = 1$ to t_{max} **do**
- 9: **for** $i = 1$ to N **do**
- 10: Select an action $a_{i,t}$ for agent λ_i
- 11: **end for**
- 12: Obtain the state s_t
- 13: Execute the joint action
 $\mathbf{a}_t = (a_{1,t}, a_{2,t}, a_{3,t}, \dots, a_{n,t})$
- 14: Obtain the new state s_{t+1} and the reward
 $\mathbf{r}_t = (r_{1,t}, r_{2,t}, r_{3,t}, \dots, r_{n,t})$
- 15: **for** $i = 1$ to N **do**
- 16: **if** Agent λ_i finish task j_k **then**
- 17: Generate coefficients α and β by generator
- 18: Obtain the revised reward $r_{i,t}^{IRL} = \alpha \cdot r_{i,t} + \beta$
- 19: **else**
- 20: Let original reward as the revised reward
 $r_{i,t}^{IRL} = r_{i,t}$
- 21: **end if**
- 22: **end for**
- 23: Store $(s_t, \mathbf{a}_t, \mathbf{r}_t, s_{t+1})$ in replay buffer \mathcal{D}
- 24: **if** The batch size of data stored in \mathcal{D} is greater than \mathcal{B} **then**
- 25: **for** $i = 1$ to N **do**
- 26: Update the agent λ_i by minimizing the loss function defined in (7) and (8)
- 27: **end for**
- 28: **end if**
- 29: **for** $i = 1$ to N **do**
- 30: **if** Agent λ_i finish task j_k **then**
- 31: Obtain the trajectory $Tra_{j_k i}$
- 32: Obtain the probability of being identified as an expert trajectory P_{ki}
- 33: Update the generator by minimizing the loss function defined in (13)
- 34: Update the discriminator by minimizing the loss function defined in (14)
- 35: **end if**
- 36: **end for**
- 37: Update the state $s_t = s_{t+1}$
- 38: **end for**
- 39: **end for**

as Algorithm 1. The generation part is primarily located in lines 15–22, where the trajectories generated by agents are optimized to gradually approach the expert trajectories. The adversarial part is mainly in lines 28–35, where adversarial learning between the generator and the discriminator is conducted, ultimately enhancing the quality of agent policies and task completion capabilities.

V. EXPERIMENT AND RESULT

In order to verify the effectiveness and efficiency of the proposed approach, experiments are conducted in the open-source multi-agent environment, which consists of agents and tasks inhabiting a two-dimensional world with continuous space and discrete time. A comparison is conducted between the proposed method and two widely used MARL algorithms, namely MASAC [37] and MAPPO [38].

A. Experiment Setup

The experiments are conducted in an open-source MARL environment developed by OpenAI. The environment consists of multiple agents interacting in a two-dimensional continuous space with discrete timesteps. The detailed environment settings are summarized in Table I.

TABLE I
ENVIRONMENT SETTINGS

Parameter	Value
Number of Agents	5 / 10 / 20
Number of Tasks	20 / 40 / 60
Environment Size	50 × 50
Speed of Agents	5
Initial Direction of Agents	Random
Timesteps Required for each Agent to Complete one Task	1
Reward for Completing a Task	7.5
Time Consumption Penalty	0.5
Energy Consumption Penalty	1.5

The hyperparameters of the proposed algorithm, including the learning rate, batch size and exploration strategy, are listed in Table II. The experiments are performed on a system equipped with an AMD Ryzen 9 5950X CPU, 32GB RAM, and an Nvidia RTX 3080Ti GPU.

TABLE II
HYPERPARAMETERS

Parameter	Value
Number of Training Episodes N_{max}	2000
Number of Steps in an Episode t_{max}	300
Learning Rate of Actors η^a	5×10^{-5}
Learning Rate of Critics η^c	10^{-5}
Discount Factor γ	0.95
Batch Size \mathcal{B}	2048
Replay Buffer \mathcal{D}	10^6
Number of Heads H	16
Model Dimensionality d_H of MHSA Mechanism	256
Learning Rate of Generator η^g	10^{-5}
Learning Rate of Discriminator η^d	2×10^{-5}

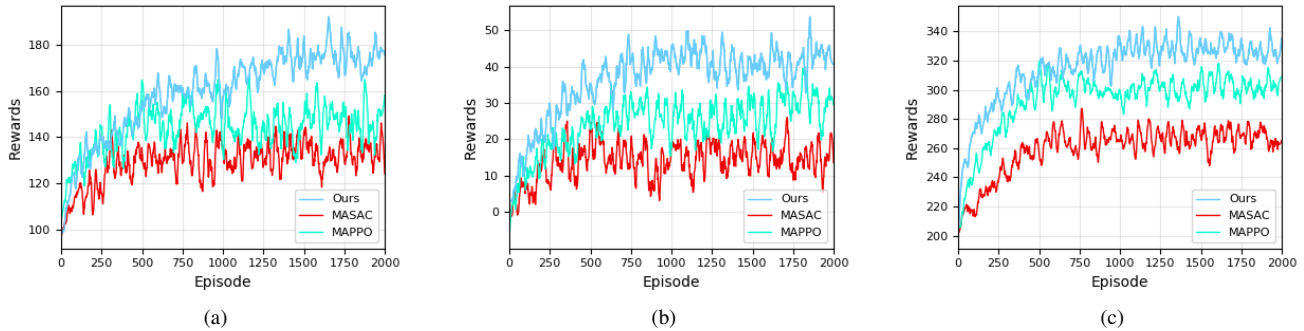


Fig. 4. Performance of time-step consumption. (a) Normal reward. (b) Sparse reward. (c) Dense reward.

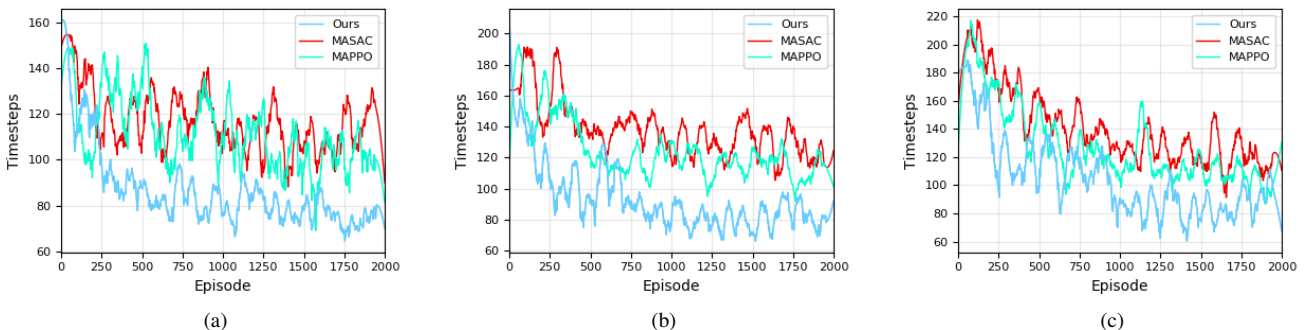


Fig. 5. Performance of time-step consumption. (a) Normal reward. (b) Sparse reward. (c) Dense reward.

To provide expert demonstrations for the IRL framework, expert trajectories were generated using a classical optimization-based task allocation algorithm under a fully static environment. Although such optimization methods are computationally expensive and thus not feasible in dynamic environments due to real-time constraints and inherent unpredictability, structured and high-quality trajectories suitable for reward inference can still be produced. These trajectories were then used to guide the IRL-based learning in more general scenarios.

B. Performance Analysis

In this subsection, experiments are conducted using the aforementioned environment settings and hyper-parameters. The performance of the proposed method is assessed based on two key metrics: the global cumulative reward and the number of consumed timesteps. These metrics collectively capture both the effectiveness and efficiency of the approach. The global cumulative reward quantifies overall performance by summing the rewards of all agents from the initial state to the completion of the final task, thereby providing a holistic measure of the method’s capability to optimize long-term rewards across the entire multi-agent system. Conversely, the number of consumed timesteps serves as an indicator of computational efficiency, where a lower value signifies accelerated convergence and enhanced coordination among agents. The integration of these two metrics enables a comprehensive

evaluation, ensuring a balanced assessment of both the quality of learning and the efficiency of execution.

Fig. 4 illustrates the performance of global cumulative rewards under different reward densities, including normal reward in Fig. 4a, sparse reward in Fig. 4b and dense reward in Fig. 4c. The proposed IRL-based method is compared against two widely used reinforcement learning algorithms, MASAC and MAPPO. The x-axis represents the number of training episodes, while the y-axis indicates the cumulative rewards obtained by the agents. Across all three settings, our proposed approach consistently outperforms the baselines, achieving higher cumulative rewards and demonstrating superior learning efficiency.

Under the normal reward setting, all three algorithms exhibit an upward trend, indicating effective policy learning. However, the proposed IRL-based method achieves significantly higher rewards than MASAC and MAPPO, suggesting better capture of the underlying reward structure and optimization of long-term returns. MAPPO performs slightly better than MASAC due to its robustness in policy updates.

The advantage of the proposed method becomes more evident under the sparse reward setting, where infrequent and delayed feedback makes learning challenging. As shown in Fig. 4b, MASAC and MAPPO struggle with lower rewards, indicating inefficient exploration. In contrast, the IRL-based method steadily improves, demonstrating its ability to infer optimal behaviors despite limited explicit rewards.

In the dense reward setting, where frequent rewards provide

TABLE III
PERFORMANCE COMPARISON OF DIFFERENT REWARD SITUATIONS.

Reward situation	Algorithm	Average reward	Avg. timestep consumption
Normal Reward	Ours	174.07	74.06
	MAPPO	147.20	102.99
	MASAC	123.85	114.90
Sparse Reward	Ours	43.19	80.19
	MAPPO	30.99	111.04
	MASAC	15.02	119.33
Dense Reward	Ours	326.95	80.15
	MAPPO	302.60	104.44
	MASAC	266.58	117.79

stronger supervision, all methods perform better. However, the proposed approach maintains the highest cumulative rewards with a more stable learning curve. MAPPO benefits from dense feedback but does not surpass IRL, while MASAC remains the weakest performer, likely due to its reliance on entropy regularization, which is less effective in this setting.

Fig. 5 illustrates time-step consumption under different reward densities: normal reward in Fig. 5a, sparse reward in Fig. 5b and dense reward in Fig. 5c. The proposed method is compared against MASAC and MAPPO, where the x-axis represents the number of timesteps required to complete the task and the y-axis denotes the corresponding reward. Across all settings, the proposed method consistently reduces task completion time, demonstrating higher efficiency than the baselines.

Under varying reward densities, the proposed IRL-based method consistently achieves lower time-step consumption compared to MASAC and MAPPO, indicating more efficient movement optimization. In the normal reward setting, the IRL-based approach steadily reduces time usage, while MASAC and MAPPO show more fluctuations, with MAPPO performing slightly better due to its stable policy updates. In the sparse reward setting, where learning is more challenging, the proposed method further outperforms the baselines. Despite similar time-step consumption, MASAC and MAPPO exhibit large differences in cumulative rewards. MAPPO tends to adopt a conservative strategy to avoid movement penalties, while MASAC maintains high exploration, resulting in more penalties and reduced rewards. In the dense reward setting, all methods benefit from frequent feedback, but the proposed method still achieves the lowest time consumption, effectively balancing task efficiency and reward maximization. The gap between MAPPO and MASAC remains small due to their similar need to trade off between movement and idleness penalties.

Table III presents the average performance metrics over 100 episodes during the execution phase under different reward densities, corresponding to varying task densities. While the variance across episodes is relatively large due to the stochastic nature of the environment and agent initialization, the performance trends remain consistent and robust across different set-

TABLE IV
PERFORMANCE COMPARISON OF DIFFERENT AGENT POPULATION.

Agent population	Algorithm	Average reward	Avg. timestep consumption
Low Number	Ours	122.50	164.20
	MAPPO	102.11	173.01
	MASAC	92.48	188.27
Medium Number	Ours	175.31	79.29
	MAPPO	150.48	111.17
	MASAC	136.65	120.32
High Number	Ours	243.07	42.67
	MAPPO	211.24	54.44
	MASAC	183.85	62.90

tings. The results show that the proposed method consistently achieves the highest average rewards and the lowest average time-step consumption across all reward settings.

Under the normal reward condition, our method achieves an average reward of 174.07 with only 74.06 timesteps, significantly outperforming MAPPO and MASAC, both of which require more steps and yield lower rewards. In the sparse reward setting, where limited feedback makes learning more challenging, the advantage becomes even more pronounced: our method delivers nearly 40% higher rewards than MAPPO and almost triple that of MASAC, while consuming fewer timesteps. In the dense reward case, although all methods improve due to frequent feedback, our method still leads with the highest reward of 326.95 and the lowest time usage of 80.15, effectively balancing reward maximization and task efficiency.

To evaluate scalability and coordination, further experiments are conducted with 40 fixed tasks and varying agent numbers (5, 10, 20). Cumulative rewards and time-step consumption are shown in Fig. 6 and Fig. 7, respectively.

In the 5-agent scenario, as shown in Fig. 6a, all methods exhibit relatively slow growth in cumulative reward due to limited parallelism and restricted task coverage. Nevertheless, the proposed method consistently achieves higher cumulative rewards throughout training, demonstrating effective policy learning even under constrained agent capacity.

As the number of agents increases to 10 in Fig. 6b, all methods show performance improvements. The proposed method maintains a more pronounced advantage over the baselines, indicating enhanced coordination and better utilization of additional agent resources. The IRL-based framework allows for more efficient learning of cooperative behaviors, leading to faster and more stable convergence.

In the 20-agent case, depicted in Fig. 6c, the reward gap widens further. The proposed method achieves the highest cumulative rewards with minimal variance, confirming its robustness and scalability in high-density multi-agent environments, where effective coordination is more challenging.

Similar trends can be observed in time-step consumption. In the 5-agent case, as shown in Fig. 7a, the limited number of agents leads to higher time-step usage across all methods.

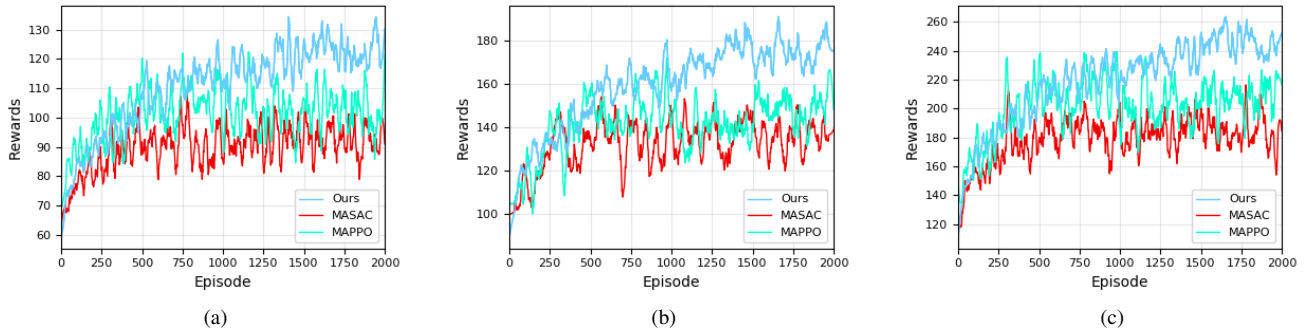


Fig. 6. Performance of cumulative reward. (a) Low number. (b) Medium number. (c) High number.

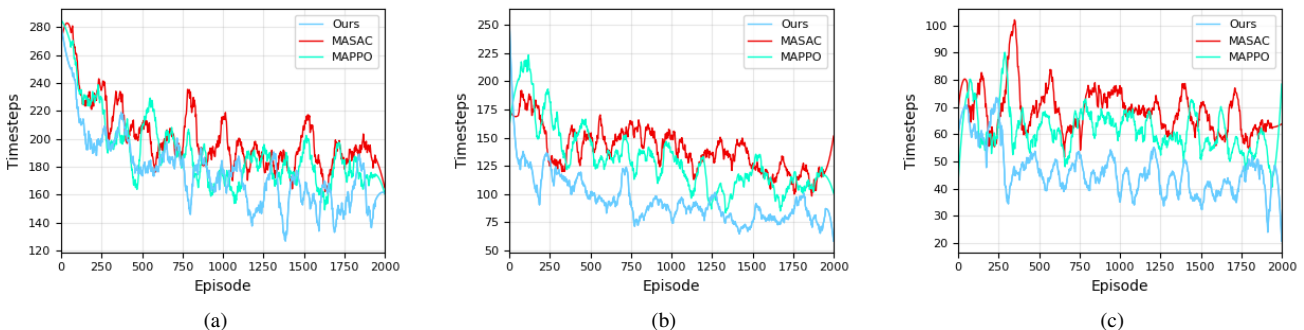


Fig. 7. Performance of time-step consumption. (a) Low number. (b) Medium number. (c) High number.

However, the proposed method demonstrates lower consumption and smoother convergence. With 10 agents in Fig. 7b, overall time usage decreases, and our method continues to show superior efficiency and stability. In the 20-agent scenario, shown in Fig. 7c, the proposed method achieves the most efficient task completion, while MASAC and MAPPO display increased fluctuations, likely due to coordination difficulties arising from higher agent density.

Table IV presents the average performance over the episodes during the execution phase under different agent population levels. The proposed method consistently achieves both higher cumulative rewards and lower time-step consumption across low, medium and high agent densities. Despite the stochastic nature of multi-agent learning environments, the performance trends remain stable and robust across different random seeds.

In the low agent population setting, performance across all methods is limited due to restricted task coverage and reduced parallelism. Nonetheless, the proposed method still outperforms the baselines, achieving an average reward of 122.50 with fewer timesteps than MAPPO and MASAC. As the agent number increases to a medium level, the gap becomes more pronounced. The proposed method not only achieves higher rewards but also improves task efficiency, completing tasks with 79.29 timesteps on average—about 30% fewer than MAPPO and MASAC. In the high agent population setting, where coordination complexity increases, the proposed method continues to lead, achieving the highest reward of 243.07 and the lowest time consumption of 42.67.

While MAPPO and MASAC also benefit from increased agent resources, their performance gains are limited by less efficient coordination mechanisms.

These results confirm that the proposed method scales effectively with different reward densities and agent numbers. It maintains strong performance in both cumulative reward and task efficiency, while demonstrating robust coordination and adaptability across a wide range of agent densities.

C. Ablation Analysis

To assess the contributions of different components in the proposed framework, ablation experiments are conducted by selectively removing key elements and analyzing their impact on performance. Specifically, the effects of removing global observations, agent trajectory information, and expert trajectories along with the generative adversarial framework are systematically examined. The corresponding results are presented in Fig. 8.

When global observations are excluded, agents must rely solely on local trajectory information, resulting in a noticeable decline in cumulative rewards. This outcome suggests that global observations provide critical contextual cues that facilitate coordinated behavior among agents. Nevertheless, the presence of trajectory-based learning still allows for a degree of adaptation, albeit less effectively.

Further performance degradation is observed when agent trajectory processing is removed. In this case, policies trained only with global observations and expert demonstrations lack

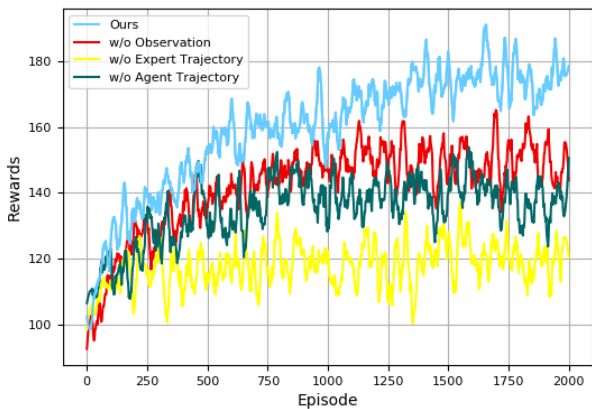


Fig. 8. Ablation Experiment Results.

direct access to the agents’ own past actions. This absence restricts the policy’s ability to make informed and adaptive decisions over time, thereby reducing both flexibility and stability in dynamic environments.

The most significant performance drop occurs when expert trajectories and the generative adversarial framework are entirely removed, forcing the model to rely exclusively on environmental rewards for training. Without the guidance of imitation learning, the training process becomes less stable, convergence is substantially slower, and the resulting policies tend to be suboptimal.

Overall, the removal of expert trajectories and the generative adversarial framework has the most detrimental effect on performance. In contrast, eliminating global observations or agent trajectory inputs still permits a certain level of learning but with diminished efficiency. These results underscore the foundational importance of the GAIL component in stabilizing training and enhancing policy quality, while also highlighting the complementary roles that global observations and agent trajectories play in supporting effective multi-agent decision-making.

D. Complexity Analysis

Consider a training scenario with n agents, m tasks, and a batch size of \mathcal{B} . In the DRL part, the complexity of the network is linearly related to the number of agents n , batch size \mathcal{B} , network dimensions and the number of layers. Since the network parameters in DRL are fixed, the complexity is $O(n\mathcal{B})$. In the generator part, the complexity of MHSA is related to the trajectory length L , feature dimensions, number of attention heads, batch size \mathcal{B} and the number of layers. With fixed network parameters, the complexity is $O(\mathcal{B}L^2)$. The complexity of the graph attention network is related to the number of nodes $n + m$, batch size \mathcal{B} and feature dimensions. With fixed network parameters, the complexity is $O(\mathcal{B}(n + m))$. In the discriminator part, since the network is a simple FCN, the complexity with fixed network parameters is $O(\mathcal{B})$. Therefore, the total complexity of the proposed algorithm is $O(n\mathcal{B} + m\mathcal{B} + \mathcal{B}L^2)$.

VI. CONCLUSION

This paper introduces a novel IRL-based MATA framework, which integrates trajectory representation learning from GAIL with a global state modeling module based on graph attention networks. Specifically, agent trajectories are encoded using a MHSA mechanism to capture temporal dependencies, while global agent-task relations are modeled through the graph attention mechanism to enhance coordination. These features are jointly processed within a generative adversarial structure to infer reward coefficients, enabling more flexible and informative policy learning without relying on manually designed reward functions. Experimental results validate the superiority of the proposed method over well-recognized baselines in terms of both cumulative reward and task efficiency. Overall, this framework offers a modular and scalable solution for cooperative multi-agent decision-making, effectively bridging domain expertise with autonomous policy learning in multi-agent systems. To further enhance the generality and applicability of the proposed framework, future work will focus on extending the method to heterogeneous agents and tasks, as well as incorporating dynamic graph structures to better capture real-world vehicular communication constraints and coordination challenges in intelligent transportation and connected vehicle systems.

VII. ACKNOWLEDGMENT

This work was supported in part by a national science foundation and by an international industry partner. The authors also appreciate the contributions from colleagues involved in the collaborative research center on intelligent systems.

REFERENCES

- [1] J. Wang, Y. Hong, J. Wang, J. Xu, Y. Tang, Q.-L. Han, and J. Kurths, “Cooperative and competitive multi-agent systems: From optimization to games,” *IEEE/CAA Journal of Automatica Sinica*, vol. 9, no. 5, pp. 763–783, 2022.
- [2] J. Orr and A. Dutta, “Multi-agent deep reinforcement learning for multi-robot applications: A survey,” *Sensors*, vol. 23, no. 7, p. 3625, 2023.
- [3] A. W. Palmer, A. J. Hill, and S. J. Scheduling, “Modelling resource contention in multi-robot task allocation problems with uncertain timing,” in *2018 IEEE International Conference on Robotics and Automation (ICRA)*. IEEE, 2018, pp. 3693–3700.
- [4] J. Ota, “Multi-agent robot systems as distributed autonomous systems,” *Advanced engineering informatics*, vol. 20, no. 1, pp. 59–70, 2006.
- [5] G. M. Skaltsis, H.-S. Shin, and A. Tsourdos, “A review of task allocation methods for uavs,” *Journal of Intelligent & Robotic Systems*, vol. 109, no. 4, p. 76, 2023.
- [6] K.-S. Kim, H.-Y. Kim, and H.-L. Choi, “A bid-based grouping method for communication-efficient decentralized multi-uav task allocation,” *International Journal of Aeronautical and Space Sciences*, vol. 21, pp. 290–302, 2020.
- [7] F. Zhang, “Intelligent task allocation method based on improved qpso in multi-agent system,” *Journal of ambient intelligence and humanized computing*, vol. 11, no. 2, pp. 655–662, 2020.
- [8] G. A. Korsah, A. Stentz, and M. B. Dias, “A comprehensive taxonomy for multi-robot task allocation,” *The International Journal of Robotics Research*, vol. 32, no. 12, pp. 1495–1512, 2013.
- [9] G. M. Skaltsis, H.-S. Shin, and A. Tsourdos, “A survey of task allocation techniques in mas,” in *2021 International Conference on Unmanned Aircraft Systems (ICUAS)*. IEEE, 2021, pp. 488–497.
- [10] N. Seenu, K. C. RM, M. Ramya, and M. N. Janardhanan, “Review on state-of-the-art dynamic task allocation strategies for multiple-robot systems,” *Industrial Robot: the international journal of robotics research and application*, vol. 47, no. 6, pp. 929–942, 2020.

- [11] G. Dulac-Arnold, N. Levine, D. J. Mankowitz, J. Li, C. Paduraru, S. Goyal, and T. Hester, "Challenges of real-world reinforcement learning: definitions, benchmarks and analysis," *Machine Learning*, vol. 110, no. 9, pp. 2419–2468, 2021.
- [12] J.-J. Wu and K.-S. Tseng, "Learning spatial search using submodular inverse reinforcement learning," in *2020 IEEE International Symposium on Safety, Security, and Rescue Robotics (SSRR)*. IEEE, 2020, pp. 7–14.
- [13] A. Shamsoshoara, F. Lotfi, S. Mousavi, F. Afghah, and İ. Güvenç, "Joint path planning and power allocation of a cellular-connected uav using apprenticeship learning via deep inverse reinforcement learning," *Computer Networks*, vol. 254, p. 110789, 2024.
- [14] D. Liu, L. Dou, R. Zhang, X. Zhang, and Q. Zong, "Multi-agent reinforcement learning-based coordinated dynamic task allocation for heterogeneous uavs," *IEEE Transactions on Vehicular Technology*, vol. 72, no. 4, pp. 4372–4383, 2022.
- [15] C. Xu and W. Song, "Intelligent task allocation for mobile crowdsensing with graph attention network and deep reinforcement learning," *IEEE Transactions on Network Science and Engineering*, vol. 10, no. 2, pp. 1032–1048, 2023.
- [16] S. Gronauer and K. Diepold, "Multi-agent deep reinforcement learning: a survey," *Artificial Intelligence Review*, vol. 55, no. 2, pp. 895–943, 2022.
- [17] Z. Zhang, X. Jiang, Z. Yang, S. Ma, J. Chen, and W. Sun, "Scalable multi-robot task allocation using graph deep reinforcement learning with graph normalization," *Electronics*, vol. 13, no. 8, p. 1561, 2024.
- [18] A. Gong, K. Yang, J. Lyu, and X. Li, "A two-stage reinforcement learning-based approach for multi-entity task allocation," *Engineering Applications of Artificial Intelligence*, vol. 136, p. 108906, 2024.
- [19] S. Paul, P. Ghassemi, and S. Chowdhury, "Learning scalable policies over graphs for multi-robot task allocation using capsule attention networks," in *2022 International Conference on Robotics and Automation (ICRA)*. IEEE, 2022, pp. 8815–8822.
- [20] M. Wang, S. Xie, X. Luo, Y. Li, H. Zhang, and H. Yu, "Hcta: Hierarchical cooperative task allocation in multi-agent reinforcement learning," in *2023 IEEE 35th International Conference on Tools with Artificial Intelligence (ICTAI)*. IEEE, 2023, pp. 934–941.
- [21] Y. Lv, J. Lei, and P. Yi, "A local information aggregation based multi-agent reinforcement learning for robot swarm dynamic task allocation," *arXiv preprint arXiv:2411.19526*, 2024.
- [22] K. Shibata, T. Jimbo, T. Odashima, K. Takeshita, and T. Matsubara, "Learning locally, communicating globally: Reinforcement learning of multi-robot task allocation for cooperative transport," *IFAC-PapersOnLine*, vol. 56, no. 2, pp. 11 436–11 443, 2023.
- [23] L. Ratnabala, A. Fedoseev, R. Peter, and D. Tsetserukou, "Magnnet: Multi-agent graph neural network-based efficient task allocation for autonomous vehicles with deep reinforcement learning," *arXiv preprint arXiv:2502.02311*, 2025.
- [24] X. Liu, Y. Wang, H. Gao, E. C. Ngai, B. Zhang, C. Wang, and W. Wang, "A coverage-aware task allocation method for uav-assisted mobile crowd sensing," *IEEE Transactions on Vehicular Technology*, 2024.
- [25] L. Ratnabala, R. Peter, A. Fedoseev, and D. Tsetserukou, "Hippo-mat: Decentralized task allocation using graphsage and multi-agent deep reinforcement learning," *arXiv preprint arXiv:2503.07662*, 2025.
- [26] Z. Fang, T. Ma, J. Huang, Z. Niu, and F. Yang, "Efficient task allocation in multi-agent systems using reinforcement learning and genetic algorithm," *Applied Sciences*, vol. 15, no. 4, p. 1905, 2025.
- [27] B. Lian, V. S. Donge, F. L. Lewis, T. Chai, and A. Davoudi, "Data-driven inverse reinforcement learning control for linear multiplayer games," *IEEE Transactions on Neural Networks and Learning Systems*, vol. 35, no. 2, pp. 2028–2041, 2022.
- [28] J.-J. Wu and K.-S. Tseng, "Adaptive submodular inverse reinforcement learning for spatial search and map exploration," *Autonomous Robots*, vol. 46, no. 2, pp. 321–347, 2022.
- [29] M. N. Azadani and A. Boukerche, "Hierarchical transformers for motion forecasting based on inverse reinforcement learning," *IEEE Transactions on Vehicular Technology*, 2024.
- [30] K. P. Sivakumar, Y. Shen, Z. Bell, S. Nivison, B. Chen, and M. M. Zavlanos, "Inverse reinforcement learning from non-stationary learning agents," *arXiv preprint arXiv:2410.14135*, 2024.
- [31] H. Sun, A. Hüyük, and M. van der Schaar, "Query-dependent prompt evaluation and optimization with offline inverse rl," *arXiv preprint arXiv:2309.06553*, 2023.
- [32] T. Freihaut and G. Ramponi, "On feasible rewards in multi-agent inverse reinforcement learning," *arXiv preprint arXiv:2411.15046*, 2025, available at <https://arxiv.org/abs/2411.15046>.
- [33] D. Waelchli, P. Weber, and P. Koumoutsakos, "Discovering individual rewards in collective behavior through inverse multi-agent reinforcement learning," *arXiv preprint arXiv:2305.10548*, 2023.
- [34] D. Goktas, A. Greenwald, S. Zhao, A. Koppel, and S. Ganesh, "Efficient inverse multiagent learning," *arXiv preprint arXiv:2502.14160*, 2025.
- [35] S. Arora and P. Doshi, "A survey of inverse reinforcement learning: Challenges, methods and progress," *Artificial Intelligence*, vol. 297, p. 103500, 2021.
- [36] J. Ho and S. Ermon, "Generative adversarial imitation learning," *Advances in neural information processing systems*, vol. 29, 2016.
- [37] S. Gupta and A. Dukkipati, "Probabilistic view of multi-agent reinforcement learning: A unified approach," 2019.
- [38] C. Yu, A. Velu, E. Vinitzky, J. Gao, Y. Wang, A. Bayen, and Y. Wu, "The surprising effectiveness of ppo in cooperative, multi-agent games," *arXiv preprint arXiv:2103.01955*, 2022, available: <https://arxiv.org/abs/2103.01955>.